Euro. Jnl of Applied Mathematics (2019), *vol.* 30, *pp.* 39–62. © Cambridge University Press 2017
doi:10.1017/S0956792517000377

Periodic pulsating dynamics of slow–fast delayed systems with a period close to the delay†

P. KRAVETC[1], D. RACHINSKII[1] and A. VLADIMIROV[2,3]

[1]*Department of Mathematical Sciences, The University of Texas at Dallas, Richardson, TX, USA*
email: pxk142530@utdallas.edu, dmitry.rachinskiy@utdallas.edu
[2]*Weierstrass Institute, Mohrenstr. 39, 10117 Berlin, Germany*
email: vladimir@wias-berlin.de
[3]*Lobachevsky State University of Nizhny Novgorod, Nizhny Novgorod, Russia*

(*Received 7 December 2016; revised 3 December 2017; accepted 4 December 2017; first published online 22 December 2017*)

We consider slow–fast delayed systems and discuss pulsating periodic solutions, which are characterised by specific properties that (a) the period of the periodic solution is close to the delay, and (b) these solutions are formed close to a bifurcation threshold. Such solutions were previously found in models of mode-locked lasers. Through a case study of population models, this work demonstrates the existence of similar solutions for a rather wide class of delayed systems. The periodic dynamics originates from the Hopf bifurcation on the positive equilibrium. We show that the continuous transformation of the periodic orbit to the pulsating regime is simultaneous with multiple secondary almost resonant Hopf bifurcations, which the equilibrium undergoes over a short interval of parameter values. We derive asymptotic approximations for the pulsating periodic solution and consider scaling of the solution and its period with the small parameter that measures the ratio of the time scales. The role of competition for the realisation of the bifurcation scenario is highlighted.

Key words: Population dynamics, bifurcation theory, singular perturbations, functional-differential equations

1 Introduction

A delay is generally believed to be a destabilising factor in population dynamics models [25]. Increasing delay can lead to oscillations where the system with zero or small delay exhibits a globally stable equilibrium. In particular, periodic pulsating solutions characterised by the alternation of time intervals of almost complete extinction of some species and outbursts in their number are typical for population dynamics (including Lotka–Volterra, host-parasite, and susceptible-infective-recovered models), chemical kinetics, and laser dynamics [8, 12]. Further, such dynamics often include processes with different time scales.

In many applications the period of the periodic pulsating solution and the delay time do not correlate. Hutchinson's delayed logistic model is a classical example of this scenario [11]. However, for certain systems, solutions with a period τ, which is close to

† P.K. and D.R. acknowledge the support of NSF through Grant DMS-1413223.

the delay time T, can play an important role. For instance, the prototype delayed model that was proposed in [30] demonstrates stable periodic regimes with $\tau \approx T$ for certain parameters of the feedback. This model has applications in lasers [6, 9, 29], population epidemics [37, 38], and malaria infection [26]. A related example is presented by the Pyragas method for non-invasive stabilisation of unstable periodic solutions to ordinary differential systems [10,18,34]. This technique uses a delayed feedback control proportional to the difference $x(t-T)-x(t)$ with T close to the period of the targeted periodic solution $x_*(t)$. The resulting stabilised periodic solution is close to x_* and therefore has a period $\tau \approx T$.

Mode-locked lasers present one further example of periodic dynamics with $\tau \approx T$, which is directly related to the subject of this work.

Mode locking of lasers [17] is used to produce periodic sequences of short optical pulses at high repetition rates, which are suitable for various applications including material processing, medical imaging, telecommunications [20, 21], optical sampling, microwave photonics, optical division multiplexing [7], and two-photon imaging [23]. The optical spectrum of a mode-locked laser consists of a set of equally spaced narrow lines corresponding to the longitudinal cavity modes characterised by fixed phase relationships between them[1]. There are two main methods to produce mode-locked optical pulses, active and passive mode-locking, and also a combination thereof called hybrid mode-locking. In particular, a passively mode-locked laser is a self-oscillating system that does not require the use of an external radio frequency modulation[2]. In the classical theory of a mode-locked laser due to Haus [16], a slow evolution of the shape of the optical pulse circulating in the cavity is described by a complex parabolic master equation of Ginzburg–Landau type. The solution describing a solitary pulse is explicit and has a hyperbolic secant profile. However, the Haus master equation is derived under the assumption of small gain and loss per cavity round trip. An alternative multi-rate functional differential model, which is free from this approximation, has been obtained from the travelling wave model in the case of a ring geometry of the laser cavity in [41]. Under further natural assumptions, such as the Lorentzian profile of the spectral filtering element, the functional differential model simplifies to the delay differential system

$$\begin{aligned}
\gamma^{-1}\dot{A}(t) &= -A(t) + \sqrt{\kappa}\exp\left(\tfrac{1}{2}\left[(1-i\eta_g)G(t-T) - (1-i\eta_q)Q(t-T)\right]\right)A(t-T),\\
\dot{Q}(t) &= q_0 - \gamma_q Q(t) - \tfrac{1}{E_q}\left(1-e^{-Q(t)}\right)|A(t)|^2,\\
\dot{G}(t) &= g_0 - \gamma_g G(t) - \tfrac{1}{E_g}e^{-Q(t)}(e^{G(t)}-1)|A(t)|^2,
\end{aligned} \tag{1.1}$$

where the complex-valued variable A is the electric field envelope at the entrance of the absorber section; $|A|^2$ represents the optical power (which is proportional to the density of photons); the real-valued variables Q and G represent integral losses and gain, respectively

[1] Achieving such phase relationships can be, at least qualitatively, viewed as a problem of synchronisation of many non-linear coupled oscillators with frequencies close to multiples of a fundamental frequency.

[2] Passive mode-locking is commonly achieved by including a saturable absorber section into the laser cavity.

https://doi.org/10.1017/S0956792517000377 Published online by Cambridge University Press

(Q and G are functions of the density of the electric charge carriers in the absorber section and the active section of the laser, respectively); the delay T stands for the cold cavity round-trip time; $\gamma \gg 1$ is the parameter of the Lorentzian profile of spectral filtering; the other parameters are explained in [41–43]. This delay differential model is suitable for describing mode-locking in a laser with large gain and losses, which is the situation typical of semiconductor laser devices[3]. At the same time, the model is amenable to analytical and numerical bifurcation analysis [1–3, 15, 19, 28, 31, 32, 40, 44]. The fundamental mode locked regime is described by a periodic pulsating solution with a period $\tau \approx T$.

The subject of this paper is a case study of a rather broad class of population models, which have a stable periodic pulsating solution with a period close to the delay time. Our goal is to highlight those features of the systems that can support the existence of such periodic solutions. These features are shared by the laser dynamics model in [41] and the population models considered here. In particular, we are interested in a bifurcation scenario associated with the formation of periodic pulses. We will use asymptotic analysis as a tool for identifying and obtaining asymptotic approximations for the periodic pulsating solution of period $\tau \approx T$.

More specifically, we consider models involving populations of species that evolve on different time scales. The models include an explicit delay time T that can have different nature and, therefore, can appear in different terms of the equations [36]; the maturity delay is considered as the main example [4, 13, 45]. We are interested in periodic dynamics presented by a limit cycle with the following properties:

(1) The period of the cycle is close to the delay time T;

(2) The time trace of one component (which we call the A-component) of the cycle is a sequence of identical short pulses, typically one pulse per period, separated by intervals where the A-component is close to zero;

(3) The oscillations are self-excited, i.e., the cycle is either globally stable or has a large basin of attraction, while the equilibrium with the zero A-component is unstable.

These properties will be formalised and quantified in terms of the parameter $\gamma \gg 1$ that measures the ratio of the slow and fast time scales of the population processes involved in the system. In particular, the period of the cycle is $T + O(1/\gamma)$, the duration of the pulse scales as $1/\gamma$, while the pulse amplitude is asymptotically proportional to γ, and the time average of each population tends to a finite positive limit value as γ increases.

In the systems that we consider, periodic solutions with the above properties are formed near a transcritical bifurcation point (threshold) separating the domain where the equilibrium with the zero A-component is stable from the domain where it is unstable and coexists with the positive equilibrium. The cycle branches from the positive equilibrium via a Hopf bifurcation and continuously transforms into periodic pulsations of the amplitude $O(\gamma)$ over a short interval of the parameter values. Therefore, we look at the bifurcations that the equilibrium points undergo near the threshold. An asymptotic analysis of the spectrum shows that there is a sequence of eigenvalues, which have almost the same real part and the imaginary parts close to the multiples of the fundamental frequency $2\pi/T$.

[3] In the limit of small gain and losses per cavity round trip, one recovers the Haus hyperbolic secant pulse shape in the delay differential model.

https://doi.org/10.1017/S0956792517000377 Published online by Cambridge University Press

Because of this, the positive equilibrium undergoes a cascade of almost simultaneous and almost resonant Hopf bifurcations in an immediate vicinity of the threshold. This cascade is simultaneous with the fast transition from a steady state to the periodic pulsating dynamics with a period $\tau \approx T$.

We take advantage of the pulsating profile of the solution to derive an asymptotic approximation to the pulses and determine their parameters using the method of matched inner (fast) and outer (slow) expansions [22]. This method was successfully applied to derive fixed-point conditions for the existence of pulsating solutions [14, 29, 38] and their asymptotics [35, 42] for both lasers and population models (however, we do not consider the existence problem here). Further, we obtain the law of scaling of pulses with γ and an equation for the pulse profile by adapting the approach used in [41]. All the asymptotic formulae are compared with numerical simulations. We also note an alternative perturbation technique of the fixed-point analysis based on averaging, which was proposed in [5].

The paper is organised as follows. In Section 2, we introduce a population model, perform a linear stability analysis of both the zero and positive steady states near the threshold, and discuss the bifurcations that initiate the pulsating dynamics. Further, the role of the competition for the realisation of the bifurcation scenario is highlighted. In Section 3, we derive asymptotic approximations for the pulsating periodic solutions. The last section contains further discussion and conclusions.

2 Bifurcation analysis

2.1 Model

We consider the system

$$\gamma^{-1}A' = -A + \kappa G(t-T)A(t-T) - \mu QA, \tag{2.1}$$

$$\gamma_q^{-1}Q' = q_0 - \beta Q - sAQ, \tag{2.2}$$

$$G' = g_0 - \alpha G - kAG, \tag{2.3}$$

where the real variables A, Q, G are population densities of three species; T is the maturity delay of the species A, see [36]; and all the parameters are positive[4]. The species A is a predator for the prey G; the species Q competes with A.

The rate of population processes for the three species is assumed to be different with A being the fastest species (with faster metabolism, higher reproductive rate, etc.), G being the slowest species, and Q changing at an intermediate rate, that is $1 \leqslant \gamma_q \leqslant \gamma$. Further, the species A is assumed to be much faster than the species G, thus $\gamma \gg 1$. The species G and Q can have comparable rates ($\gamma_q \approx 1$) or Q can be much faster than G ($1 \ll \gamma_q$). However, it is important to stress that the parameters γ and γ_q play different roles in the following asymptotic analysis. Namely, our asymptotic formulae are obtained in the limit of $\gamma \to \infty$ while we keep γ_q fixed. In numerical simulations, we use γ_q ranging from 1 to γ.

[4] The death rate of the species A is scaled to 1. The number of parameters can be further reduced in a standard way by rescaling the phase variables and time.

https://doi.org/10.1017/S0956792517000377 Published online by Cambridge University Press

The species Q plays an important role, which will be clarified in further sections. In particular, we will see that the system of the two equations (2.1) (with zero Q) and (2.3) does not demonstrate pulsating dynamics near the threshold.

The species Q and G are assumed to be recruited through constant immigration in equations (2.1)–(2.3). In further sections, we will show that similar systems with different recruitment terms, including recruitment with constant birth rate, show similar pulsating dynamics near the threshold. Also, delaying different terms has little effect on solutions in our examples; for instance, replacing the delayed term $G(t-T)$ by $G(t)$ in equations (2.1)–(2.3) preserves the periodic pulsating dynamics.

We will discuss non-negative solutions only. Note that system (2.1)–(2.3), as well as all the other systems considered in the paper, is positively invariant.

We associate the pulsating regime of system (2.1)–(2.3) near the point of the transcritical bifurcation of equilibria with the Hopf bifurcations from the positive equilibrium. The recruitment rate g_0 of the prey G will be used as the bifurcation parameter.

2.2 Bifurcations at the equilibrium with $A = 0$

System (2.1)–(2.3) has an equilibrium with zero A,

$$A_o = 0, \qquad Q_o = \frac{q_0}{\beta}, \qquad G_o = \frac{g_0}{\alpha}, \tag{2.4}$$

for all positive g_0, and a positive equilibrium either for $g_0 > g_0^*$ or for $g_0 < g_0^*$, where the threshold value g_0^* is defined by

$$\frac{\kappa g_0^*}{\alpha} - \frac{\mu q_0}{\beta} = 1. \tag{2.5}$$

These two equilibria collide in a transcritical bifurcation for $g_0 = g_0^*$. The positive equilibrium near the threshold is defined by the asymptotic formulae

$$A_* = \tilde{a}\delta + O(\delta^2), \qquad Q_* = \frac{q_0}{\beta} + \tilde{q}\delta + O(\delta^2), \qquad G_* = \frac{g_0^*}{\alpha} + \tilde{g}\delta + O(\delta^2), \tag{2.6}$$

where $\delta = g_0 - g_0^*$ and the coefficients of the first order correction are given by

$$\tilde{a} = \frac{1}{\dfrac{kg_0^*}{\alpha} - \dfrac{\alpha\mu s q_0}{\kappa\beta^2}}, \qquad \tilde{q} = \frac{1}{\dfrac{\alpha\mu}{\kappa} - \dfrac{kg_0^*\beta^2}{\alpha s q_0}}, \qquad \tilde{g} = \frac{\mu}{\kappa}\tilde{q}.$$

We will assume that

$$\frac{kg_0^*}{\alpha^2} > \frac{\mu s q_0}{\kappa\beta^2}. \tag{2.7}$$

In this case, the positive equilibrium exists for $g_0 > g_0^*$ and is stable near the threshold. (If the opposite inequality holds, then the positive equilibrium exists for $g_0 < g_0^*$ and is unstable near the threshold.)

https://doi.org/10.1017/S0956792517000377 Published online by Cambridge University Press

The eigenvalues of the linearisation of system (2.1)–(2.3) at the equilibrium (2.4) with zero A are defined by the relations $\lambda = -\gamma\beta < 0$, $\lambda = -\alpha < 0$ and

$$1 + \frac{\lambda}{\gamma} = \frac{\kappa g_0}{\alpha} e^{-\lambda T} - \frac{\mu q_0}{\beta}. \tag{2.8}$$

The solutions of equation (2.8) satisfy $\operatorname{Re}\lambda < 0$ in a left neighbourhood of the threshold, more precisely, for $g_0 < g_0^* = \alpha(1 + \mu q_0/\beta)/\kappa$. Hence, the equilibrium (2.4) is stable below the threshold, i.e., for $g_0 < g_0^*$. Consequently, the positive equilibrium (2.6) is stable in a small right neighbourhood of the threshold, i.e., for small $\delta = g_0 - g_0^* > 0$.

The equilibrium (2.4) undergoes a sequence of Hopf bifurcations in a small right neighbourhood of the threshold $g_0 = g_0^*$ for large γ. To see this, first note that in the limit $\gamma = \infty$ the solutions of the characteristic equation (2.8) have the form

$$\lambda = i\omega_n, \qquad \omega_n = \frac{2\pi n}{T}, \qquad n = 1, 2, \ldots,$$

i.e., the equilibrium satisfies the necessary condition for infinitely many simultaneous Hopf bifurcations at the threshold point $g_0 = g_0^*$. Moreover, these bifurcations are in resonance with each other as the frequencies ω_n are all multiples of $2\pi/T$. For finite γ, setting $\lambda = i\omega$ in (2.8) in order to satisfy the Hopf bifurcation condition, and rearranging, we obtain the equations

$$\frac{\omega}{\gamma} = -\frac{\kappa g_0^*}{\alpha} \tan \omega T, \tag{2.9}$$

$$\delta = g_0^* \left(\frac{1}{\cos \omega T} - 1 \right) > 0, \tag{2.10}$$

which define the frequency of the cycle and the bifurcation value of the parameter $g_0 = g_0^* + \delta$ for each Hopf bifurcation from the equilibrium (2.4). Figure 1 illustrates solutions of the transcendental equation (2.9). For $\gamma \gg 1$, the solutions of equations (2.9) and (2.10) are approximated by the asymptotic formulae

$$\omega_n = \frac{2\pi n}{T} \left(1 - \frac{\alpha}{\kappa g_0^* \gamma T} + \frac{\alpha^2}{\left(\kappa g_0^* \gamma T\right)^2} \right) + O\left(\gamma^{-3}\right), \tag{2.11}$$

$$\delta_n = \frac{\alpha^2}{2\kappa^2 g_0^*} \left(\frac{2\pi n}{\gamma T} \right)^2 + O\left(\gamma^{-3}\right) \tag{2.12}$$

with $n = 1, 2, \ldots$ Hence, the n-th Hopf bifurcation after the threshold has a frequency close to $2\pi n/T$ and $O(\sqrt{\gamma})$ Hopf bifurcations occur within the distance of order $1/\gamma$ from the threshold on the parameter g_0 axis.

Following [24, 47], the spectrum of the zero equilibrium defined by equation (2.8) can be called *weak* or *pseudocontinuous* spectrum. It is characterised by a specific scaling of the real and imaginary parts of the eigenvalues $\lambda = x + i\gamma\omega$ with $\gamma \gg 1$, where x and ω are of order 1. Using this scaling, we obtain from (2.8) an approximate relationship

https://doi.org/10.1017/S0956792517000377 Published online by Cambridge University Press

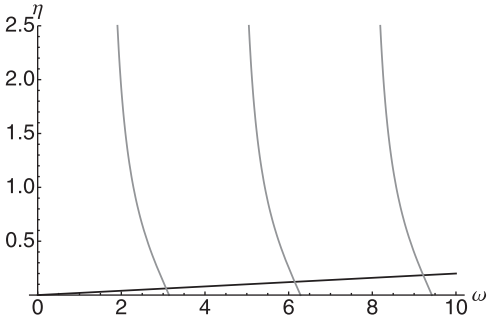

FIGURE 1. Solution of equation (2.9). The horizontal axis is ω. Every second intersection of the straight line $\eta = \omega/\gamma$ and the function $\eta = -\kappa g_0^* \tan(\omega T)/\alpha$ satisfies the condition (2.10). Here $\gamma = 100$, $T = 1$.

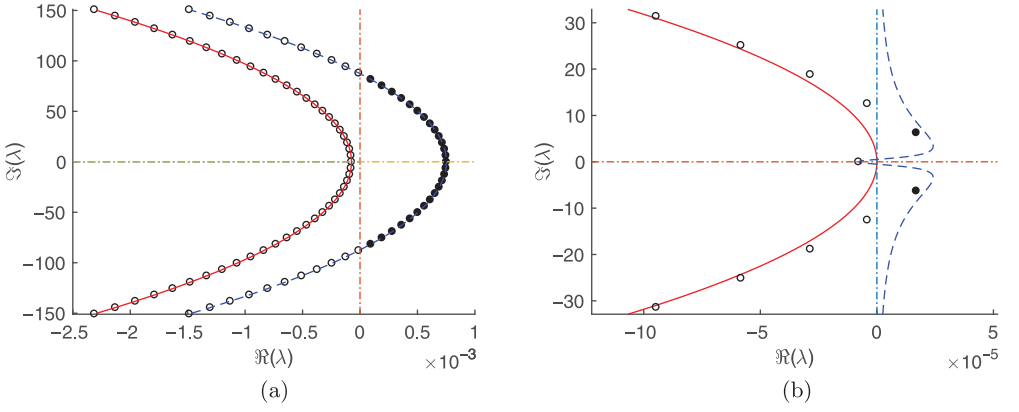

FIGURE 2. Panel (a): Spectra of the zero equilibrium for $g_0 = 3.7497$ and $g_0 = 3.7528$. Numerical values of the eigenvalues are shown by circles; lines are obtained from equation (2.13). Filled circles correspond to unstable eigenvalues. Panel (b): Spectrum of the positive equilibrium of system (2.1)–(2.3) after the first Hopf bifurcation ($g_0 = 3.75003$), i.e., exactly one pair of complex conjugate eigenvalues cross the imaginary axis from left to right. Solid line defined by (2.19) carries the weak spectrum; dashed line (2.18) carries the strong spectrum. Parameters are as follows: $\gamma = 1,000$, $\gamma_q = 10$, $\kappa = 0.6$, $\mu = 0.5$, $\alpha = 1$, $q_0 = 2.5$, $\beta = 1$, $s = 1$, $k = 0.7$, $T = 1$.

between the real and imaginary parts of the eigenvalues:

$$x(\omega) = \frac{1}{2T}\left(2\ln\left(\frac{g_0}{g_0^*}\right) - \ln\left(1 + \left(\frac{\alpha\omega}{g_0^*\kappa}\right)^2\right)\right) + O(\gamma^{-1}), \tag{2.13}$$

which is dual to formulae (2.11) and (2.12). The curve (2.13) carrying the eigenvalues simply moves to the right with increasing g_0, see Figure 2(a).

2.3 Bifurcations at the positive equilibrium

As the bifurcation parameter g_0 increases across the threshold, the positive equilibrium (2.6) also undergoes a sequence of Hopf bifurcations, which we deem responsible for the

https://doi.org/10.1017/S0956792517000377 Published online by Cambridge University Press

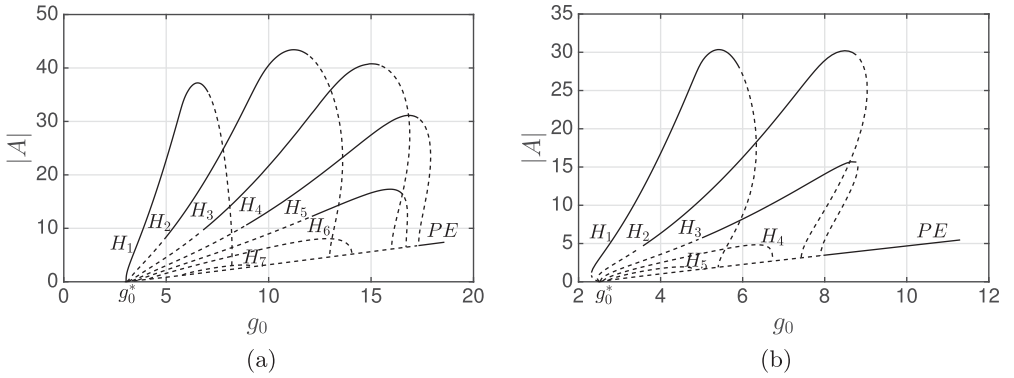

FIGURE 3. Bifurcation diagrams obtained with numerical package DDE-BIFTOOL for system (2.1)–(2.3) for two parameter sets. The vertical axis shows the maximum of the A-component of a periodic solution. The PE line corresponds to the positive equilibrium. Branches H_1–H_7 (H_1–H_5 on panel (b)) correspond to the periodic solutions born via Hopf bifurcations on the positive equilibrium. Stable branches are shown by solid lines and unstable branches are shown by dashed lines. The branch H_1 on panel (b) exhibits slight hysteresis near the threshold g_0^*. All the branches connect to the branch of the positive equilibrium at Hopf bifurcation points at both ends.

creation and formation of the periodic pulsating solution. The first Hopf bifurcation with the frequency close to $2\pi/T$ destabilises the positive equilibrium and creates a stable cycle (see branch H_1 in Figure 3). As the parameter g_0 increases further, this cycle changes its shape continuously into a pulsating periodic solution, see Figure 4. The amplitudes of harmonics of the A-component $A(t/\tau) = \sum_{n=1}^{\infty} A_n \cos(2\pi n t/\tau + \phi_n)$ of the periodic solution, where τ is the period of A, grow with g_0, while the phase differences $\phi_k - \phi_1$ almost vanish, see Figure 5. At the same time, the positive equilibrium undergoes a cascade of secondary Hopf bifurcations with the frequencies of the higher harmonics. The whole cascade of the Hopf bifurcations and the transformation of the cycle to a pulsating solution happen in a small right neighbourhood of the threshold $g_0 = g_0^*$, see Figure 5.

The characteristic equation for the positive equilibrium is

$$e^{T\lambda} = \frac{G_* \kappa (\alpha + \lambda)\left(A_* s \gamma_q + \beta \gamma_q + \lambda\right)}{(A_* k + \alpha + \lambda)\left(A_* s \gamma_q \left(1 + \frac{\lambda}{\gamma}\right) + (\beta \gamma_q + \lambda)\left(1 + \frac{\lambda}{\gamma} + Q_* \mu\right)\right)}. \tag{2.14}$$

Using asymptotic formulae (2.6) and the ansatz $\lambda = i\omega$ for the eigenvalues of the linearisation, we obtain the following asymptotic formulae for the frequency and the bifurcation value of the parameter at each Hopf bifurcation point[5]:

$$\omega_n = \frac{2\pi n}{T}\left(1 - \frac{\alpha}{\kappa g_0^* \gamma T}\right) + O\left(\gamma^{-2}\right), \tag{2.15}$$

[5] The term of order γ^{-2} in the expansion (2.15) is different from the corresponding term in the expansion (2.11).

https://doi.org/10.1017/S0956792517000377 Published online by Cambridge University Press

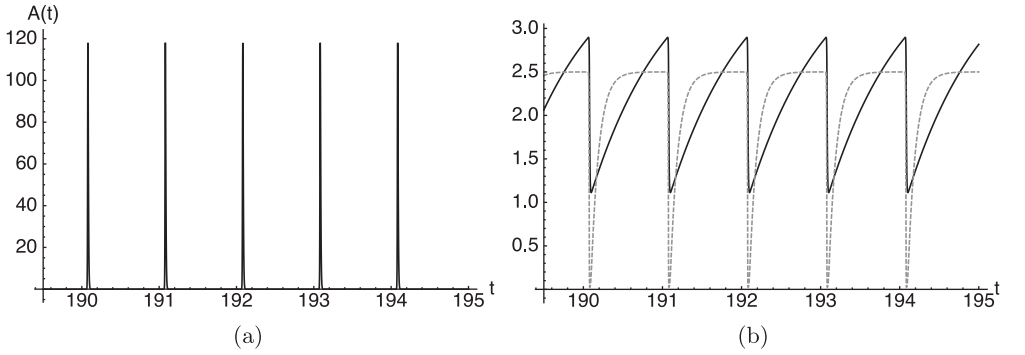

FIGURE 4. Time trace of the periodic solution of system (2.1)–(2.3). Panel (a): The A-component. Panel (b): The G-component (solid) and the Q-component (dashed). The A-component is almost zero between the pulses. The Q-component almost reaches the equilibrium value $q_0/\beta = 2.5$ between the pulses of the A-component and drops almost to zero during the pulse because $\gamma_q = 10$ is relatively large. The G-component drops fast during the pulse and then recovers slowly between the pulses. The period of the solution is close to the delay $T = 1$. The following parameters were used: $\gamma = 400$, $\gamma_q = 10$, $\kappa = 0.6$, $g_0 = 4$, $q_0 = 2.5$, $\alpha = 1$, $\beta = 1$, $s = 1$, $k = 0.7$, $T = 1$. The threshold value is $g_0^* = 3.75$.

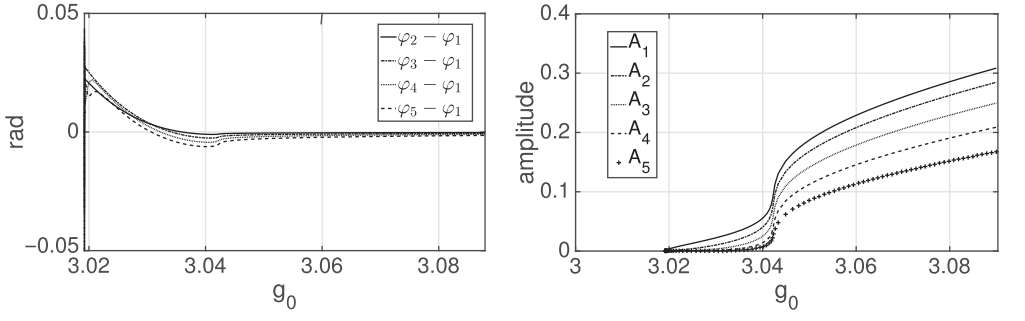

FIGURE 5. The phase and amplitude of the Fourier coefficients for the A-component $A(t/\tau) = \sum_{n=1}^{\infty} A_n \cos(2\pi n t/\tau + \phi_n)$ of the periodic solution along the branch H_1 shown in Figure 3(a), where τ is the period of solution.

$$\delta_n = \left(\frac{2\pi n}{\gamma T}\right)^2 \frac{\left(\beta^2 g_0^* \kappa k - \alpha^2 \mu q_0 s\right)\left(\beta^2 + \left(\frac{2\pi n}{T\gamma_q}\right)^2\right)}{2\kappa^2 g_0^* \beta^2 \left(\mu q_0 s - g_0^* \kappa k \left(\frac{\beta^2 + \left(\frac{2\pi n}{T\gamma_q}\right)^2}{\alpha^2 + \left(\frac{2\pi n}{T}\right)^2}\right)\right)} + O\left(\gamma^{-3}\right). \tag{2.16}$$

We assume that, along with the relation (2.7), the conditions

$$\mu q_0 s > g_0^* \kappa k \left(\frac{\beta^2 + \left(\frac{2\pi}{T\gamma_q}\right)^2}{\alpha^2 + \left(\frac{2\pi}{T}\right)^2}\right) \qquad \text{and} \qquad \gamma_q > \frac{\alpha}{\beta} \tag{2.17}$$

are satisfied. Under these conditions, relation (2.16) implies $\delta = g_0 - g_0^* > 0$ for $n = 1, 2, \ldots$ That is, according to equations (2.7) and (2.16), conditions (2.17) ensure that the positive

https://doi.org/10.1017/S0956792517000377 Published online by Cambridge University Press

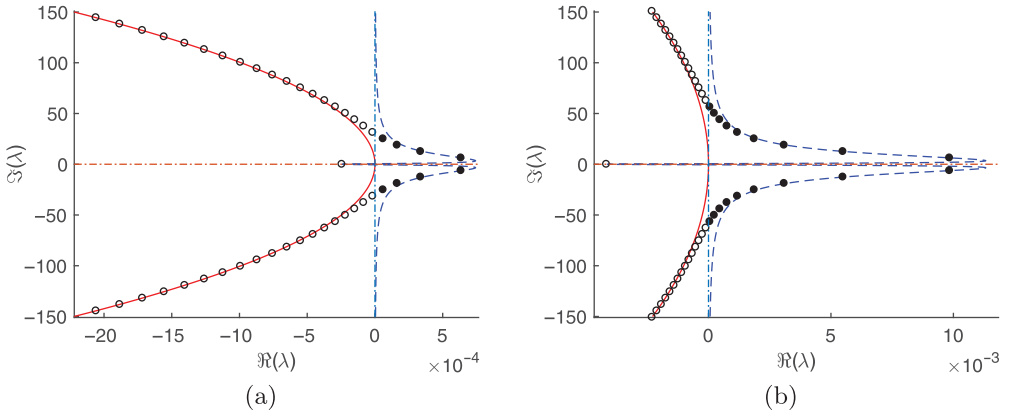

FIGURE 6. Spectrum of the positive equilibrium and curves (2.19), (2.18) for $g_0 = 3.7509$ (panel (a)) and $g_0 = 3.7648$ (panel(b)). Notation and other parameters are the same as in Figure 2(b).

equilibrium undergoes the Hopf bifurcations with the frequencies close to the multiples $2\pi n/T$ of $2\pi/T$ for $n = 1, 2, \ldots$ as g_0 increases across the threshold.

The spectrum of the positive equilibrium can be divided into two parts, which have different asymptotic properties with respect to the large parameter γ, cf. [24]. The *strong* spectrum consists of the eigenvalues $\lambda = x + i\omega + O(\gamma^{-1})$, which originate from the limit $\gamma = \infty$. Equation (2.14) implies the following approximate implicit relationship between the real and imaginary parts for these eigenvalues:

$$\frac{G_*^2\kappa^2\left((\alpha+x)^2+\omega^2\right)\left(\left(\gamma_q\left(A_*s+\beta\right)+x\right)^2+\omega^2\right)}{\left((\alpha+A_*k+x)^2+\omega^2\right)\left(\left(\gamma_q\left(A_*s+\beta+\beta\mu Q_*\right)+\mu Q_* x+x\right)^2+\left(\mu Q_*\omega+\omega\right)^2\right)} = e^{2Tx}. \tag{2.18}$$

The *weak* spectrum is characterised by the asymptotic relationship $\lambda = x + i\gamma\omega$ and satisfies the approximate relationship

$$x(\omega) = \frac{1}{2T}\ln\left(\frac{G_*^2\kappa^2}{G_*^2\kappa^2+\omega^2}\right). \tag{2.19}$$

With increasing g_0, branches of the curve (2.19) 'open'. Simultaneously, weak eigenvalues with smaller imaginary part leave this curve, cross imaginary axis producing the Hopf bifurcations described by equations (2.15) and (2.16), and become a part of the strong spectrum (2.18), see Figures 2(b) and 6.

In Table 1, the asymptotic values of ω_n and δ_n given by formulae (2.15) and (2.16) are compared with the numerical values obtained for $\gamma = 600$, $\gamma_q = 40$, $\kappa = 0.6$, $\mu = 0.5$, $\alpha = 1$, $q_0 = 2.5$, $\beta = 1$, $s = 1$, $k = 0.7$, $T = 1$. Using these parameters for numerical continuation, we observe 24 branches of periodic solutions. Table 1 features the first six branches. The accuracy of the asymptotic formulae decreases with increasing n.

We have conducted a number of further numerical simulations with different parameter sets satisfying conditions (2.7) and (2.17), and observed bifurcation diagrams and oscillating periodic solutions similar to those presented in Figures 3 and 4.

https://doi.org/10.1017/S0956792517000377 Published online by Cambridge University Press

Table 1. *Comparison of the asymptotic and numerical values of δ_n, ω_n for the following set of parameters:* $\gamma = 600$, $\gamma_q = 40$, $\kappa = 0.6$, $\mu = 0.5$, $\alpha = 1$, $q_0 = 2.5$, $\beta = 1$, $s = 1$, $k = 0.7$, $T = 1$

	$\delta_n = g_0 - g_0^*$			ω_n		
n	Asymptotic	Numerical	Error (%)	Asymptotic	Numerical	Error (%)
1	1.1177×10^{-5}	1.1170×10^{-5}	0.06	6.2785	6.2785	$< 10^{-4}$
2	4.6817×10^{-5}	4.6896×10^{-5}	0.17	12.5571	12.5571	$< 10^{-4}$
3	1.1665×10^{-4}	1.1731×10^{-4}	0.56	18.8356	18.8356	1.60×10^{-4}
4	2.3632×10^{-4}	2.3903×10^{-4}	1.13	25.1141	25.1140	3.57×10^{-4}
5	4.2773×10^{-4}	4.3593×10^{-4}	1.88	31.3927	31.3925	6.18×10^{-4}
6	7.1905×10^{-4}	7.3993×10^{-4}	2.82	37.6712	37.6708	9.45×10^{-4}

2.4 The role of competition

Here, we briefly discuss the critical role of the species Q, which competes with the fast species A, in creating the pulsating periodic dynamics via the bifurcation scenario described above.

In order to highlight the role of the Q-species, we compare the dynamics of system (2.1)–(2.3) with that of the dynamics of the system

$$\gamma^{-1} A' = -A + \kappa G(t - T) A(t - T), \tag{2.20}$$

$$G' = g_0 - \alpha G - kAG, \tag{2.21}$$

which is obtained by setting $Q = 0$ in equation (2.1) and dropping equation (2.2). Dynamics of system (2.20), (2.21) is essentially the same as dynamics of system (2.1)–(2.3) with zero immigration rate $q_0 = 0$ of the Q-species.

System (2.20), (2.21) has two equilibrium points

$$A = 0, \quad G = \frac{g_0}{\alpha}; \qquad A = \frac{\kappa(g_0 - g_0^*)}{k} = \frac{\kappa\delta}{k}, \quad G = \frac{1}{\kappa},$$

which collide in the transcritical bifurcation at the threshold value

$$g_0^* = \frac{\alpha}{\kappa} \tag{2.22}$$

of the bifurcation parameter g_0. Like in the case of the three-dimensional systems (2.1)–(2.3), the equilibrium with zero A is stable below the threshold and unstable above the threshold, while the equilibrium with non-zero A is positive and stable above the threshold, i.e., for $g_0 > g_0^*$ (without any additional assumptions about the parameters of equations (2.20) and (2.21)). The unstable equilibrium undergoes the cascade of Hopf bifurcations at the bifurcation points, and with the frequencies, defined by relations (2.9) and (2.10) and satisfying the asymptotic formulae (2.11) and (2.12). However, the positive equilibrium remains stable for all $g_0 > g_0^*$, and the system exhibits the equilibrium dynamics rather than a periodic dynamics above the threshold. The reason is that the equilibrium with

https://doi.org/10.1017/S0956792517000377 Published online by Cambridge University Press

non-zero A undergoes the cascade of Hopf bifurcations below the threshold that is in the parameter domain $g_0 < g_0^*$ where this equilibrium has a negative A-component and is unstable, rather than above the threshold where the equilibrium is positive and stable. Indeed, substituting the ansatz $\lambda = i\omega$ in the characteristic equation

$$\gamma^{-1}(\lambda + \kappa g_0)\lambda + (1 - e^{-\lambda T})\lambda + \kappa g_0 - \alpha e^{-\lambda T} = 0 \tag{2.23}$$

of the linearisation of the system at the equilibrium with non-zero A, we obtain the asymptotic formula

$$\delta = -\frac{\alpha}{2\kappa}\left(\frac{2\pi n}{\gamma T}\right)^2\left(1 + \left(\frac{2\pi n}{\alpha T}\right)^2\right) + O(\gamma^{-3}),$$

where the negative sign of $\delta = g_0 - g_0^*$ indicates that the Hopf bifurcation occurs below the threshold. Equation (2.23) implies

$$(\omega^2 + \kappa^2 g_0^2)(1 + \omega^2\gamma^{-2}) = \omega^2 + \alpha^2$$

for $\lambda = i\omega$, which is only possible for $g_0 \leqslant g_0^* = \alpha/\kappa$, that is below the threshold, thus proving stability of the positive equilibrium. Clearly (2.23) cannot have real positive eigenvalues for $g_0 > g_0^*$ either.

3 Scaling with γ: Approximate solution

3.1 Separation of slow and fast stages

In order to analyse and approximate the asymptotic behaviour of the pulsating periodic solution for large γ, we adapt the approach proposed by New and Haus for modelling optical systems in [16, 27] by partial differential equations and an extension of this approach to delay differential models of mode-locked semiconductor lasers developed in [41].

Consider a pulsating periodic solution of equations (2.1)–(2.3). We divide the period into two stages, the short fast stage $t_b \leqslant t \leqslant t_e$ containing the pulse and the slow stage $t_e \leqslant t \leqslant t_b + \tau$, during which A is close to zero. Here $\tau \approx T$ is the period of the solution, t_b is the moment when a pulse begins, t_e is the moment when the pulse ends, $t_e - t_b \ll 1$. We then further introduce a partition $t_b < t_b' < t_e' < t_e$ of the fast stage into three sub-intervals. During the interval $[t_b, t_b']$ the variable A grows from a small value ε to a large value ε^{-1}, it stays larger than ε^{-1} over the interval $[t_b', t_e']$, and decreases back to the small value ε over the interval $[t_e', t_e]$ (to be specific, $\varepsilon = \varepsilon(\gamma)$ scales with γ in such a way that $\epsilon(\gamma) \to 0$ and $-\gamma^{-1}\ln\epsilon(\gamma) \to 0$ as $\gamma \to \infty$). We assume that A grows exponentially on $[t_b, t_b']$ as $e^{\gamma\lambda_1 t}$ and exponentially decreases as $e^{\gamma\lambda_2 t}$ on $[t_e', t_e]$ with $\lambda_1 > 0 > \lambda_2$. These assumptions will be shown to lead to a self-consistent answer for the pulse (in particular the values of λ_1 and λ_2 are evaluated below). Further, they imply that

$$G(t_b) \approx G(t_b'), \qquad Q(t_b) \approx Q(t_b'), \qquad \int_{t_b}^{t_e} A(\theta)\,d\theta \approx \int_{t_b'}^{t_e'} A(\theta)\,d\theta \tag{3.1}$$

https://doi.org/10.1017/S0956792517000377 Published online by Cambridge University Press

for large γ (that is, the left and right sides of each relation in (3.1) have the same limit as $\gamma \to \infty$). This allows us to identify t_b with t_b' and t_e with t_e' in the asymptotic approximations below.

Finally, we assume that the period of the periodic solution scales with γ as

$$\tau = T\left(1 + \frac{c}{\gamma T}\right) + O(\gamma^{-2}), \tag{3.2}$$

which again proves to lead to consistent asymptotic approximations.

3.2 Area of the pulse

During the phase $[t_b', t_e']$ of the pulse of A, the terms AQ and AG in the Q and G equations are large compared to the other terms, which therefore can be neglected. Hence, during this phase, equations (2.2) and (2.3) can be approximated by the following equations:

$$\begin{aligned} \gamma_q^{-1} Q' &= -sAQ, \\ G' &= -kAG. \end{aligned}$$

Integrating these equations and using the approximations (3.1), we obtain for the full fast stage $[t_b, t_e]$:

$$Q(t) = Q(t_b')e^{-\gamma_q s \int_{t_b'}^{t} A(\theta)\,d\theta} \approx Q_b e^{-\gamma_q s P(t)}, \qquad G(t) = e^{-k\int_{t_b'}^{t} A(\theta)\,d\theta} \approx G_b e^{-kP(t)}, \tag{3.3}$$

where $Q_b = Q(t_b)$, $G_b = G(t_b)$ and

$$P(t) = \int_{t_b}^{t} A(\theta)\,d\theta. \tag{3.4}$$

In particular, for the values $G(t_e) = G_e$, $Q_e = Q(t_e)$ at the moment $t = t_e$, we have

$$G_e = G_b e^{-kp}, \qquad Q_e = Q_b e^{-\gamma_q sp}, \tag{3.5}$$

where

$$p = \int_{t_b}^{t_e} A(\theta)\,d\theta.$$

On the other hand, integrating equation (2.1) over the fast stage and using the fact that A is close to zero at the moments t_b and t_e, we obtain the approximate equation

$$p = \kappa \int_{t_b - T}^{t_e - T} G(\theta)A(\theta)\,d\theta - \mu \int_{t_b}^{t_e} Q(\theta)A(\theta)\,d\theta. \tag{3.6}$$

The exponential form of the pulse that we assumed on the subintervals $[t_b, t_b']$ and $[t_e', t_e]$ of the fast stage and the estimate $\tau - T = O(\gamma^{-1})$ for the small difference between the period and the delay, which follows from (3.2), imply that $\int_{t_b-T}^{t_e-T} G(\theta)A(\theta)\,d\theta \approx \int_{t_b-\tau}^{t_e-\tau} G(\theta)A(\theta)\,d\theta$. Hence, the integrals in the right-hand side of equation (3.6) are essentially integrals over the fast stage for two successive pulses. Therefore, using the periodicity of the solution

https://doi.org/10.1017/S0956792517000377 Published online by Cambridge University Press

and relations (3.3), we can rewrite equation (3.6) approximately as

$$p = \kappa \int_{t_b-\tau}^{t_e-\tau} G(\theta)A(\theta)\,d\theta - \mu \int_{t_b}^{t_e} Q(\theta)A(\theta)\,d\theta$$
$$= \int_{t_e}^{t_b} \left(\kappa\, G_b e^{-kP(\theta)} - \mu\, Q_b e^{-\gamma_q s P(\theta)}\right) A(\theta)\,d\theta.$$

Further, using equation (3.4), $A(\theta)\,d\theta = d\,P(\theta)$; hence,

$$p = \frac{\kappa G_b}{k}(1 - e^{-kp}) - \frac{\mu Q_b}{\gamma_q s}(1 - e^{-\gamma_q sp}). \tag{3.7}$$

During the slow stage, the terms AQ and AG are small compared to the other terms in the Q and G equations. Neglecting these terms results in the linear equations

$$\gamma_q^{-1} Q' = q_0 - \beta Q,$$
$$G' = g_0 - \alpha G.$$

Integrating these equations over the slow stage $[t_e, t_b + \tau]$ and combining the integrals

$$g_0 - \alpha G_b = (g_0 - \alpha G_e)e^{-\alpha(t_b+\tau-t_e)} \approx (g_0 - \alpha G_e)e^{-\alpha T},$$

$$q_0 - \beta Q_b = (q_0 - \beta Q_e)e^{-\gamma_q \beta(t_b+\tau-t_e)} \approx (q_0 - \beta Q_e)e^{-\gamma_q \beta T}$$

with equation (3.5), we obtain

$$G_b = \frac{g_0(1 - e^{-\alpha T})}{\alpha(1 - e^{-\alpha T - kp})}, \qquad Q_b = \frac{q_0(1 - e^{-\gamma_q \beta T})}{\beta(1 - e^{-\gamma_q \beta T - \gamma_q sp})}. \tag{3.8}$$

Hence, equation (3.7) implies the fixed-point condition

$$p = \frac{\kappa g_0(1 - e^{-\alpha T})(1 - e^{-kp})}{k\alpha(1 - e^{-\alpha T - kp})} - \frac{\mu q_0(1 - e^{-\gamma_q \beta T})(1 - e^{-\gamma_q sp})}{\gamma_q s\beta(1 - e^{-\gamma_q \beta T - \gamma_q sp})} =: \eta(p). \tag{3.9}$$

The right-hand side $\eta(p)$ is zero at zero, has the derivative $\kappa g_0/\alpha - \mu q_0/\beta > 1$ at zero, and converges to a constant as $p \to \infty$, see Figure 7(a). Therefore, equation (3.9) has a positive root. Under further assumptions, the positive root is unique. For instance, the uniqueness is guaranteed whenever we increase the parameter γ_q keeping all the other parameters in equation (3.9) fixed. In particular, the positive root is unique in all the examples below. The conclusion is that the integral of the A-component over a period converges to a positive root p_* of equation (3.9) as $\gamma \to \infty$ (with other parameters fixed).

Figure 7(b) compares the value $p(\gamma)$ of this integral with its limit value p_*. The integral has been evaluated numerically for 40 values of γ from the interval $100 \leqslant \gamma \leqslant 4,000$ by direct simulation of equations (2.1)–(2.3). The power law fit

$$\phi(\gamma) = \hat{p}_* + b\gamma^{-v}$$

was used to obtain the estimate $\hat{p}_*$ of the limit value p_* of the integral. For the parameter set in Figure 7b, the error between the numerical estimate $\hat{p}_*$ and the analytic value of $p_* = 0.492$ obtained from equation (3.9) satisfies $|p_* - \hat{p}_*| < 10^{-3}$.

https://doi.org/10.1017/S0956792517000377 Published online by Cambridge University Press

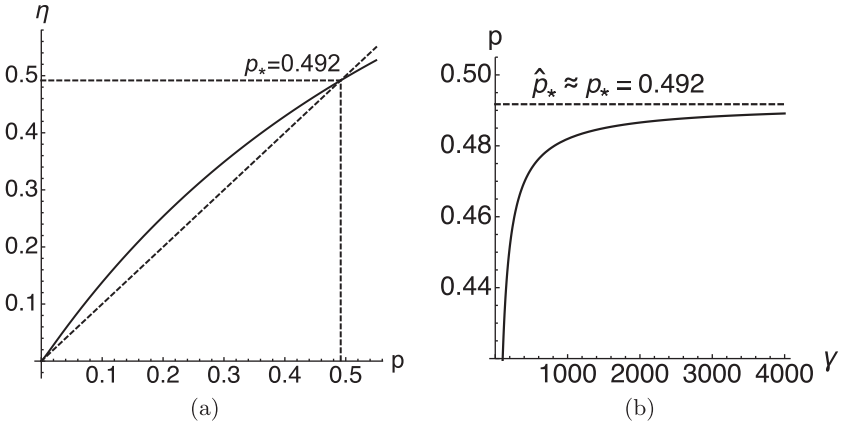

FIGURE 7. Panel (a) shows the solution of equation (3.9). Panel (b) shows the dependence of the integral of A-component of system (2.1)–(2.3) over one period on γ. The power law fit is shown by the solid line. The horizontal asymptote $p = \hat{p}_*$ coincides with analytic value p_* shown on panel (a). Here, $\kappa = 0.6$, $\mu = 0.5$, $\alpha = 1$, $q_0 = 1$, $\beta = 1$, $s = 2$, $k = 1$, $T = 1$, $\gamma_q = 100$, $g_0 = 2.6$.

We conclude that in the limit of γ tending to infinity, the component A of the periodic solution converges to the periodic sequence of delta functions (Dirac comb),

$$A \to p_* \sum_{n=-\infty}^{\infty} \delta(t - nT), \tag{3.10}$$

which has the period T equal to the delay. The component G grows according to the equation $G' = g_0 - \alpha G$ from the value $G_e = G_b e^{-kp_*}$ to the value G_b defined by equation (3.8), i.e.,

$$G(t) = \frac{g_0}{\alpha} - \left(\frac{g_0}{\alpha} - G_e\right) e^{-\alpha(t-nT)}, \qquad nT < t < (n+1)T,$$

between the pulses of A, and drops back to the value G_e during the pulse. Similarly, the component Q is as approximated between the pulses as

$$Q(t) = \frac{q_0}{\beta} - \left(\frac{q_0}{\beta} - Q_e\right) e^{-\gamma_q \beta(t-nT)}, \qquad nT < t < (n+1)T.$$

The interval $g_0^* < g_0 < g_0^* + \varepsilon$ of the parameter values, over which the cycle born via Hopf bifurcation on the positive equilibrium transforms to the pulsating solution, collapses to the threshold, that is $\varepsilon \to 0$, as γ grows to infinity. In other words, the pulsating solution described by equation (3.10) can be found 'immediately' beyond the threshold for large γ.

3.3 Pulse shape

The above approximation does not provide information about the fast stage of the solution such as the profile of the pulse or the deviation of the period from the delay T. In order to obtain such information, one can adapt the approach of Haus and its modifications, see [16, 41]. We briefly outline a possible approach without going into much detail. This approach gives us the law of scaling of the pulse shape and the period with γ.

https://doi.org/10.1017/S0956792517000377 Published online by Cambridge University Press

Using the periodicity of the solution and the asymptotic formula (3.2) for the period, we can rewrite equation (2.1) as

$$\gamma^{-1}A'(t) + A(t) + \mu Q(t)A(t) = \kappa G(t + c\gamma^{-1})A(t + c\gamma^{-1}).$$

Integrating this equation from t_b over a part of the fast stage $t_b \leqslant t \leqslant t_e$, using the approximations (3.1) and $P(t_b + c\gamma^{-1}) \approx 0$, and taking into account that $A(t_b) \approx 0$, we obtain an approximate equation

$$\gamma^{-1}A(t) + \int_{t_b}^{t} A(\theta)\,d\theta + \mu Q_b \int_{t_b}^{t} e^{-\gamma_q s P(\theta)} A(\theta)\,d\theta = \kappa G_b \int_{t_b + c\gamma^{-1}}^{t + c\gamma^{-1}} e^{-kP(\theta)} A(\theta)\,d\theta.$$

As $A = P'$, we obtain, similarly to equation (3.7),

$$\gamma^{-1}P'(t) + P(t) + \frac{\mu Q_b}{\gamma_q s}(1 - e^{-\gamma_q s P(t)}) = \frac{\kappa G_b}{k}(1 - e^{-kP(t + c\gamma^{-1})}), \tag{3.11}$$

where G_b, Q_b are defined by equation (3.8) with $p = p_*$ being a positive root of equation (3.9). Introducing the fast and reversed time scale $\theta = -\gamma t$, and changing the variable $\bar{P}(\theta) = P(t - c\gamma^{-1})$, we rewrite equation (3.11) as

$$-\bar{P}'(\theta) + \bar{P}(\theta) + \frac{\mu Q_b}{\gamma_q s}(1 - e^{-\gamma_q s \bar{P}(\theta)}) = \frac{\kappa G_b}{k}(1 - e^{-k\bar{P}(\theta - c)}), \tag{3.12}$$

where G_b, Q_b are defined from equations (3.7) and (3.8). A single pulse of the pulsating periodic solution is, therefore, described by a solution of equation (3.12) satisfying the boundary conditions

$$\bar{P}(-\infty) = p_*, \qquad \bar{P}(\infty) = 0. \tag{3.13}$$

Note that both 0 and p_* are equilibrium points of equation (3.12). Therefore, conditions (3.13) define a heteroclinic orbit of this equation. More precisely, if $\tilde{P}$ denotes the heteroclinic solution of equation (3.12) satisfying equation (3.13), and $\tilde{A} = \tilde{P}'$, then a pulse of the periodic solution of system (2.1)–(2.3) is approximated by the formula

$$A(t) = \gamma \tilde{A}(-\gamma t) = \gamma \tilde{P}'(-\gamma t) \tag{3.14}$$

for large γ. Hence, according to this approximation, the amplitude of the pulse scales linearly with γ, the width of the pulse is inverse proportional to γ, and the period is approximated by equation (3.2).

Linearising system (3.12) at 0 and p_*, we obtain

$$-P'(\theta) + (1 + \mu Q_b)P(\theta) = \kappa G_b\, P(\theta - c) \tag{3.15}$$

and

$$-P'(\theta) + (1 + \mu Q_e)P(\theta) = \kappa G_e P(\theta - c), \tag{3.16}$$

respectively, where Q_e, G_e are defined by (3.5) with $p = p_*$. The characteristic equation of linearisation (3.15) is

$$-\lambda + 1 + \mu Q_b = \kappa G_b\, e^{-\lambda c}. \tag{3.17}$$

https://doi.org/10.1017/S0956792517000377 Published online by Cambridge University Press

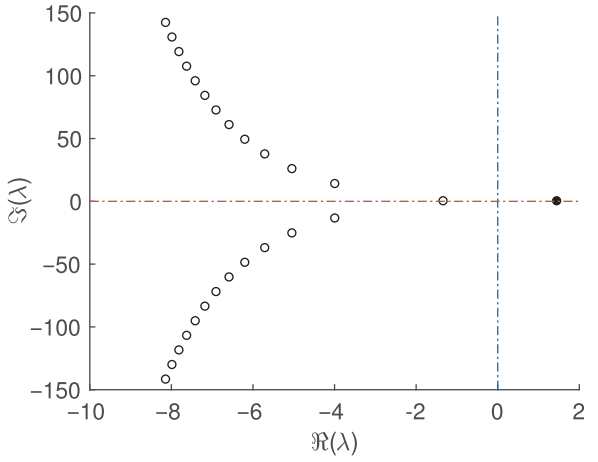

FIGURE 8. A typical spectrum of equations (3.17) and (3.18) when condition (3.19) is satisfied. The notation is the same as in Figure 2.

The characteristic equation of equation (3.16) has a similar form

$$-\lambda + 1 + \mu Q_e = \kappa G_e e^{-\lambda c}. \tag{3.18}$$

We will assume that

$$\kappa G_b - \mu Q_b - 1 < 0, \qquad \kappa G_e - \mu Q_e - 1 < 0. \tag{3.19}$$

These conditions can be associated with New's stability criterion [27], which ensures stability of the background of the pulses, that is, in our context, stability with respect to small perturbations of the A-component at the beginning and at the end of the slow stage when A is close to zero. Relations (3.19) imply that each of equations (3.17) and (3.18) has two real roots of different signs. A typical spectrum of these equations is shown in Figure 8. Here, all the complex eigenvalues have a negative real part, which is less than the real negative eigenvalue. In such a case, both equilibrium points $\bar{P} = 0$ and $\bar{P} = p_*$ of equation (3.12) are saddles with a one-dimensional unstable manifold and a codimension 1 stable manifold. Therefore, for a specific value of the parameter c, which can be considered as a bifurcation parameter in equation (3.12), the unstable manifold of the equilibrium point p_* can connect to the stable manifold of the zero equilibrium forming a heteroclinic orbit. The value of c, for which the heteroclinic orbit is formed, defines the period of the solution of system (2.1)–(2.3) according to the asymptotic formula (3.2), and the heteroclinic orbit $\tilde{P}$ defines the profile of the pulse according to (3.14). Figure 9 illustrates how the heteroclinic orbit and the corresponding c can be found by the shooting method. Further, the heteroclinic solution $\tilde{P}(\theta)$ converges to the equilibrium p_* exponentially as $e^{\lambda_+^e \theta}$ in the limit $\theta \to -\infty$, where λ_+^e is the positive real root of equation (3.18); and, to the zero equilibrium as $e^{\lambda_-^b \theta}$ in the limit $\theta \to \infty$, where λ_-^b is the negative real root of equation (3.17). Hence, equation (3.14) implies that the pulse of A has similar exponential tails. Specifically, A grows exponentially as $e^{-\gamma \lambda_-^b t}$ at the beginning of the fast stage and decays as $e^{-\gamma \lambda_+^e t}$ at the end of the fast stage. This result is consistent with the exponential

https://doi.org/10.1017/S0956792517000377 Published online by Cambridge University Press

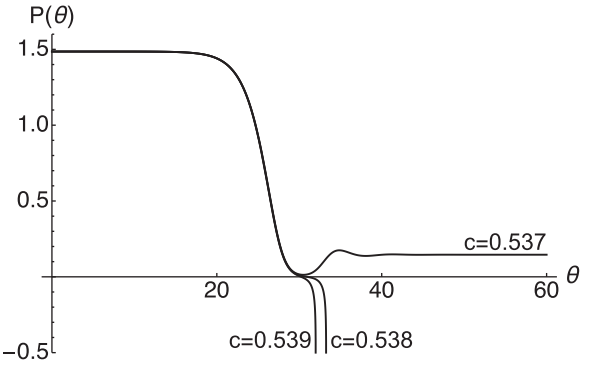

FIGURE 9. We adopt the shooting method in order to find parameter c in equation (3.12). The three curves correspond to three trajectories starting near the equilibrium $p_* = 1.486$ with different values of c. Other parameters are $G_b = 2.906$, $Q_b = 2.5$, $k = 0.7$, $\gamma_q = 10$, $s = 1$, $\mu = 0.5$, and $\kappa = 0.6$. Note that with this set of parameters, equation (3.12) has an additional positive equilibrium $p_\dagger = 0.146$ that is an asymptotically stable focus. For one exact value $c = c_*$ ($0.537 < c_* < 0.538$) there exists a heteroclinic orbit of (3.12) connecting the equilibria p_* and 0. This orbit describes the shape of the pulse, and the value c_* defines the period of the pulsating solution. For $c < c_*$, trajectories starting near p_* belong to the basin of attraction of the positive equilibrium $p_\dagger$; for $c > c_*$, such trajectories become negative and go to negative infinity.

growth assumptions that we made earlier about the pulse. In particular, the assumed exponential asymptotics of the pulse tails hold with $\lambda_1 \approx -\lambda_-^b$ and $\lambda_2 \approx -\lambda_+^e$ (cf. p. 12).

The above exponential asymptotics of the pulse tails have been derived for the phase when G and Q change fast. The same asymptotics can be obtained directly from equation (2.1) for the beginning and the end of the slow stage when G and Q change slowly. Indeed, replacing $A(t-T)$ with $A(t+c\gamma^{-1})$ according to (3.2), setting $G = G_e, Q = Q_e$ for the beginning of the slow stage and $G = G_b, Q = Q_b$ for the end of the slow stage, and using the exponential ansatz $A = A_0 e^{-\gamma\lambda t}$ corresponding to the fast evolution of A results in the same characteristic equations (3.17) and (3.18). Thus, the exponential asymptotics at the slow and fast stages match.

Figure 10 compares a pulse of the periodic solution of system (2.1)–(2.3) with the approximation obtained from the heteroclinic orbit of equation (3.12).

3.4 Approximation for $\gamma_q \gg 1$

The parameter γ_q controls the rate of the population processes for the species Q. Denote by $\tilde{p}$ the unique positive root of the equation

$$p = \frac{\kappa g_0 (1 - e^{-\alpha T})(1 - e^{-kp})}{k\alpha(1 - e^{-\alpha T - kp})}$$

(cf. (3.9)). If we increase the value of γ_q keeping the parameters in the right-hand side of equations (2.1)–(2.3) fixed, then p_*, $G_{b,e}$, $Q_{b,e}$ approach the following values:

$$p_* \approx \tilde{p}, \quad G_b \approx \frac{g_0(1 - e^{-\alpha T})}{\alpha(1 - e^{-\alpha T - k\tilde{p}})}, \quad G_e \approx G_b e^{-k\tilde{p}}, \quad Q_b \approx q_0/\beta, \quad Q_e \approx 0.$$

https://doi.org/10.1017/S0956792517000377 Published online by Cambridge University Press

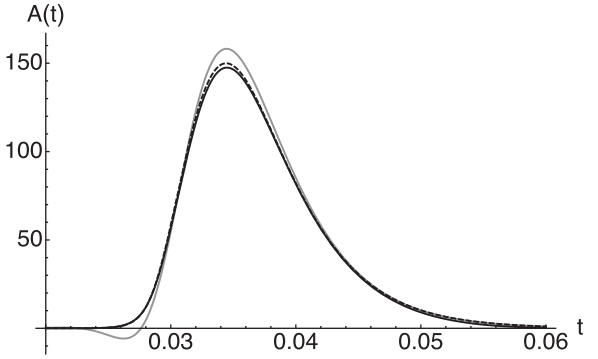

FIGURE 10. Black solid curve represents a single pulse of the A-component of the periodic pulsating solution of system (2.1)–(2.3) with the following parameters: $g_0 = 4$, $k = 0.7$, $q_0 = 2.5$, $s = 1$, $T = 1$, $\alpha = 1$, $\beta = 1$, $\gamma = 400$, $\kappa = 0.6$, $\mu = 0.5$, $\gamma_q = 100$. Dashed curve is the derivative of the heteroclinic solution of equation (3.12) satisfying the boundary conditions (3.13). This solution exists for $c = 0.3736$ that was found using the shooting method, see Figure 9. Grey solid curve is the derivative of the heteroclinic solution of the approximating equation (3.20) connecting the saddle equilibrium point $\tilde{p} = 1.6968$ and the stable focus at zero. This curve oscillates near the focus and fails to approximate the leading edge of the pulse (left tail).

Further, equation (3.12) for the pulse profile can be approximated by the equation

$$-\bar{P}'(\theta) + \bar{P}(\theta) = \frac{\kappa G_b}{k}(1 - e^{-k\bar{P}(\theta - c)}), \tag{3.20}$$

which has the equilibrium points $\bar{P} = 0$ and $\bar{P} = \tilde{p}$. Since $Q_e \approx 0$, the characteristic equation of the linearisation of equation (3.20) at the equilibrium $\bar{P} = \tilde{p}$ approximates (3.18). However, the characteristic equation $-\lambda + 1 = \kappa G_b\, e^{-\lambda c}$ of the linearisation at zero is different from (3.17). For example, one can show that if $\kappa G_b c < 1$, then the zero equilibrium of equation (3.20) is stable; at the same time, the first relation in equation (3.19) ensures that zero is a saddle for equation (3.12). This situation is illustrated in Figure 10. The heteroclinic orbit, which connects the saddle point $\tilde{p}$ with the stable zero equilibrium of equation (3.20) approximates the pulse well for the main part of the fast stage, but fails to approximate the pulse tails. The heteroclinic orbit of equation (3.12) gives a better approximation.

3.5 Pulses with unstable background

Pulsating periodic solutions with a period close to T can be obtained also when one of the conditions (3.19), or both of them, is violated. According to the classification of New [27], such pulses have unstable background. For example, consider the case when

$$\kappa G_b - \mu Q_b - 1 > 0, \qquad \kappa G_e - \mu Q_e - 1 < 0. \tag{3.21}$$

Here, the main role is played by the characteristic equation

$$-\lambda + 1 + \mu \hat{Q}(\hat{t}) = \kappa \hat{G}(\hat{t})\, e^{-\lambda c}, \qquad 0 \leqslant \hat{t} \leqslant T \tag{3.22}$$

https://doi.org/10.1017/S0956792517000377 Published online by Cambridge University Press

with $t = t_b - \hat{t}$ varying over the slow stage, where

$$\hat{G}(\hat{t}) = \frac{g_0}{\alpha} + e^{\alpha\hat{t}}\left(G_b - \frac{g_0}{\alpha}\right), \qquad \hat{Q}(\hat{t}) = \frac{q_0}{\beta} + e^{\gamma_q\beta\hat{t}}\left(Q_b - \frac{q_0}{\beta}\right),$$

and c is considered as a parameter again. To be definite, assume that for each $\hat{t}$, equation (3.21) has two real roots $\lambda_-(\hat{t}) < \lambda_+(\hat{t})$ that depend continuously on $\hat{t}$ and satisfy the relations

$$\lambda_-(\hat{t}) < \lambda_+(\hat{t}) < 0 \quad \text{for} \quad 0 \leqslant \hat{t} < t_o; \qquad \lambda_-(\hat{t}) < 0 < \lambda_+(\hat{t}) \quad \text{for} \quad t_o < \hat{t} \leqslant T, \tag{3.23}$$

which are compatible with (3.21). Further, suppose that $\operatorname{Re}\lambda < \lambda_-(\hat{t})$ for all the complex roots. Then, the zero equilibrium $\bar{P} = 0$ of equation (3.12) is stable, while the equilibrium $\bar{P} = p_*$ has a one-dimensional unstable manifold. Assuming that this unstable manifold belongs to the basin of attraction of zero, it contains a heteroclinic orbit that defines the pulse profile during the fast stage. This orbit is robust with respect to variations of the parameter c. Therefore, c (and the period (3.2)) cannot be identified as an isolated value for which the heteroclinic solution is formed (as it was the case for pulses with stable background satisfying (3.19) where the heteroclinic orbit connected saddle equilibria). Instead, c is determined by the evolution of A during the slow stage, when A is small, and the periodic solution satisfies the approximate equation

$$-\gamma^{-1}\frac{A}{d\hat{t}} = -A + \kappa\hat{G}(\hat{t})A(\hat{t} - \gamma^{-1}c) - \mu\hat{Q}(\hat{t})A.$$

The zero equilibrium of this equation exhibits the delayed loss of stability so that $A \approx A(0)e^{\gamma\lambda_+(\hat{t})}$ approaches zero very closely over an interval of time $[0, t_o]$ when $\lambda_+(\hat{t}) < 0$ (see (3.23)) and then returns to its initial value $A(T) = A(0)$ over the interval $[t_o, T]$. This allows us to predict that for the pulsating periodic solution of equations (2.1)–(2.3), in the limit $\gamma \to \infty$, one has

$$\int_0^T \lambda_+(\hat{t})\, d\hat{t} = 0. \tag{3.24}$$

Since $\lambda_+ = \lambda_+(t; c)$ depends on c, condition (3.24) selects c and defines the period (3.2).

It should be noted that condition (3.24) was not satisfied in the numerical simulations that we performed. The reason is that A gets extremely close to zero and becomes affected by numerical noise between the pulses. The effect can be understood if we replace equation (2.1) with the following equation:

$$\gamma^{-1}A' = -A + \kappa G(t - T)A(t - T) - \mu QA + \eta$$

containing a small immigration term $\eta > 0$. This modification makes sense from the modelling perspective too because it precludes A from becoming as small as $e^{-\gamma}$ between the pulses. For this equation (coupled with equations (2.2) and (2.3)), the period depends on both γ and η as we confirmed numerically. However, one can predict that the pulsating periodic solution with a period $\tau \approx T$ should disappear in the limit $\gamma \to \infty$ with a fixed η. On the other hand, if η decreases with γ as fast as $e^{-\gamma}$, pulses with the period defined by equations (3.2) and (3.24) can exist.

https://doi.org/10.1017/S0956792517000377 Published online by Cambridge University Press

4 Conclusion

We have explored a class of pulsating periodic regimes, which can evolve due to the delay, the non-linearity, and the slow–fast structure in delay differential systems. These solutions have a period close to the delay and are characterised by a specific scaling of the pulse width and height with the parameter $\gamma \gg 1$ measuring the ratio of the fast and slow time scales. Further, the periodic pulses are formed close to some threshold value of the bifurcation parameter, at which a zero equilibrium undergoes the transcritical bifurcation and a positive equilibrium appears. Through a case study of a population model, which involves a fast predator and a slow prey, we have shown that the formation of periodic pulses is simultaneous with a cascade of multiple, almost simultaneous resonant Hopf bifurcations that occur in the immediate vicinity of the threshold on the positive equilibrium. Using the asymptotic analysis at zero, we have obtained explicit relationships between the parameters, which ensure this scenario (such as (2.7) and (2.17)). In particular, we have highlighted the role of competition and shown that the pulses with the associated Hopf bifurcations appear when the fast species competes with another species; in the absence of competition, pulses do not form near the threshold[6].

The same analysis can be applied to a wider class of population models. In particular, we obtained counterparts of relationships (2.7), (2.16), and (2.17) for several variants of model (2.1)–(2.3) with different growth terms. We then confirmed numerically the same bifurcation scenario leading to the formation of pulses near the threshold. In one variation of the model, the constant immigration and linear death terms $q_0 - \beta Q$ and $g_0 - \alpha G$ in equations (2.2) and (2.3) have been replaced with the logistic terms, $Q(q_0 - \beta Q)$ and $G(g_0 - \alpha G)$, respectively. In another variant of the model,

$$\begin{aligned} \gamma^{-1} A' &= \kappa G(t-T)A(t-T) - \tau A - \mu Q A - f A^2, \\ \gamma_q^{-1} Q' &= \nu G Q - \beta Q - s A Q - r Q^2, \\ G' &= g_0 - \alpha G - k A G - m Q G, \end{aligned}$$

the A and Q species both predate on G, and the intraspecific competition is included. Interestingly, the counterpart of condition (2.7) for this system requires $\mu s > f r$ in order to guarantee that the positive equilibrium undergoes the cascade of Hopf bifurcations in a small neighbourhood of the threshold. The relation $\mu s > f r$ means that interspecific competition between the species A and Q is stronger than intraspecific competition. In the classical competing species model, this condition ensures the competitive exclusion scenario; the opposite inequality $\mu s < f r$ implies the coexistence scenario.

Using the method of matched asymptotic expansions at the slow and fast stages of the dynamics, we have obtained an approximation to the pulsating solution, which provides an accurate prediction of the area of the pulse. Furthermore, a modification of the method of Haus has allowed us to obtain asymptotics of the period and the pulse shape as $\gamma \to \infty$. This shape is described by a heteroclinic solution of a scalar delay equation that depends only on three parameters. The heteroclinic orbit connects two saddle equilibrium points, each having a one-dimensional unstable manifold.

[6] It is worth noting that the model in [30] also has a predator–prey structure. The pulses in this model, or in the models considered in this work, are not related to switching between stable branches of a critical manifold of a singularly perturbed system.

https://doi.org/10.1017/S0956792517000377 Published online by Cambridge University Press

Similar periodic pulsating solutions have been previously found in the laser model (1.1) and its variations [40,41]. The main advance of this work is a detailed asymptotic analysis of the pulses and linear stability analysis near the bifurcation point. These analyses can be extended to lasers. Some differences between population and laser models arise from the fact that population systems are positively invariant, and the pulsating regime in this setting is positive. On the other hand, the pulsating variable A in the laser model (1.1) is complex valued. Also, different types of non-linearities in population and laser models result in different power laws for the scaling of pulses with γ.

Due to positive invariance, the transcritical bifurcation with the associated zero eigenvalue is an important ingredient of the bifurcation scenario described in this work. It is interesting to compare this scenario with the Eckhaus and modulational instabilities, which are well known in the context of spatially distributed systems and have been recently studied for systems containing large delays [33,46]. The evolution of the pseudocontinuous spectrum of the zero equilibrium shown in Figure 2(a) is similar to the picture associated with the Eckhaus instability. The 'parabola' carrying the pseudocontinuous spectrum moves as a whole to the unstable half-plane as the bifurcation parameter increases. Furthermore, as in the Eckhaus scenario [39], we observe the appearance of multiple unstable periodic solutions, which then stabilise via secondary bifurcations leading to co-existence of multiple periodic attractors, see Figure 3. On the other hand, the evolution of the spectrum of the positive equilibrium that intersects the zero equilibrium in the transcritical bifurcation reminds the modulation instability scenario, in which the 'parabola' carrying the pseudocontinuous spectrum develops two humps that cross the imaginary axis, while the vertex of the parabola at zero is not moving [33]. Interestingly, although similar humps are observed in Figure 6, they are formed through a different mechanism. Namely, eigenvalues with smaller imaginary part that belong to the pseudocontinuous spectrum get absorbed by the strongly stable spectrum as the bifurcation parameter increases. This interaction of the pseudocontinuous and strongly stable spectra results in the formation of humps and, further, in stabilisation of the positive equilibrium for higher values of the bifurcation parameter. However, a common feature of all the above scenarios is that eigenvalues with smaller imaginary part cross the imaginary axis from the stable to the unstable domain before eigenvalues with larger imaginary part do. Hence, all these scenarios can be viewed as long-wavelength instabilities.

References

[1] Arkhipov, R., Pimenov, A., Radziunas, M., Rachinskii, D., Vladimirov, A. G., Arsenijevic, D., Schmeckebier, H. & Bimberg, D. (2013) Hybrid mode-locking in semiconductor lasers: Simulations, analysis and experiments. *IEEE J. Sel. Top. Quantum Electron.* **19**, 1100208.

[2] Arkhipov, R. M., Amann, A. & Vladimirov, A. G. (2015) Pulse repetition-frequency multiplication in a coupled cavity passively mode-locked semiconductor lasers. *J. Appl. Phys. B:* **118**, 539–548.

[3] Arkhipov, R. M., Habruseva, T., Pimenov, A., Radziunas, M., Huyet, G. & Vladimirov, A. G. (2016) Semiconductor mode-locked lasers with coherent dual mode optical injection: Simulations, analysis and experiment. *J. Opt. Soc. Am. B* **33**, 351–359.

[4] Banerjee, S., Mukhopadhyay, B. & Bhattacharyya, R. (2010) Effect of maturation and gestation delays in a stage structure predator prey model. *J. Appl. Math. Inform.* **28**(5–6), 1379–1393.
[5] Carr, T. W., Haberman, R. & Erneux, T. (2012) Delay-periodic solutions and their stability using averaging in delay-differential equations, with applications. *Phys. D: Nonlinear Phenom.* **241**(18), 1527–1531.
[6] Carr, T. W., Schwartz, I. B., Kim, M. Y. & Roy, R. (2006) Delayed-mutual coupling dynamics of lasers: Scaling laws and resonances. *SIAM J. Dyn. Syst.* **5**, 699–725.
[7] Delfyett, P. J., Gee, S., Choi, M.-T., Izadpanah, H., Lee, W., Ozharar, S., Quinlan, F. & Yilmaz, T. (2006) Optical frequency combs from semiconductor lasers and applications in ultrawideband signal processing and communications. *J. Lightwave Technol.* **24**(7), 2701–2719.
[8] Erneux, T. (2009) *Applied Delay Differential Equations*, Springer, Springer-Verlag, New York.
[9] Erneux, T. & Mandel, P. (1995) Minimal equations for antiphase dynamics in multimode lasers. *Phys. Rev. A* **52**, 4137–4144.
[10] Fiedler, B., Flunkert, V., Hövel, P. & Schöll, E. (2010) Delay stabilization of periodic orbits in coupled oscillator systems. *Philos. Trans. R. Soc. Lond. A: Math. Phys. Eng. Sci.* **368**, 319–341.
[11] Fowler, A. C. (1982) An asymptotic analysis of the delayed logistic equation when the delay is large. *IMA J. Appl. Math.* **28**, 41–49.
[12] Fowler, A. C. (2005) Asymptotic methods for delay equations. *J. Eng. Math.* **53**, 271–290.
[13] Gourley, S. A. & Kuang, Y. (2004) A stage structured predator-prey model and its dependence on maturation delay and death rate. *J. Math. Biol.* **49**(2), 188–200.
[14] Grigorieva, E. V. & Kashchenko, S. A. (1993) Complex temporal structures in models of a laser with optoelectronic delayed feedback. *Opt. Commun.* **102**, 183–192.
[15] Habruseva, T., Hegarty, S. P., Vladimirov, A. G., Pimenov, A., Rachinskii, D., Rebrova, N., Viktorov, E. A. & Huyet, G. (2010) Bistable regimes in an optically injected mode-locked laser. *Opt. Express* **20**, 25572–25583.
[16] Haus, H. (1975) Theory of mode locking with a slow saturable absorber. *IEEE J. Quantum Electron.* **11**(9), 736–746.
[17] Haus, H. A. (2000) Mode-locking of lasers. *IEEE J. Sel. Top. Quantum Electron.* **6**(6), 1173–1185.
[18] Hooton, E. W. & Amann, A. (2012) Analytical limitation for time-delayed feedback control in autonomous systems. *Phys. Rev. Lett.* **109**(15), 154101.
[19] Jaurigue, L., Pimenov, A., Rachinskii, D., Schöll, E., Lüdge, K. & Vladimirov, A. G. (2015) Timing jitter of passively mode-locked semiconductor lasers subject to optical feedback: A semi-analytic approach. *Phys. Rev. A* **92**, 053807.
[20] Jiang, L. A., Ippen, E. P. & Yokoyama, H. (2007) *Ultrahigh-Speed Optical Transmission Technology*, Springer, Springer-Verlag Berlin, Heidelberg.
[21] Kaiser, R. & Hüttl, B. (2007) Monolithic 40-ghz mode-locked mqw dbr lasers for high-speed optical communication systems. *IEEE J. Sel. Top. Quantum Electron.* **13**(1), 125–135.
[22] Kevorkian, J. & Cole, J. D. (1980) *Perturbation Methods in Applied Mathematics*, Springer, Springer-Verlag, New York.
[23] Kuramoto, M., Kitajima, N., Guo, H., Furushima, Y., Ikeda, M. & Yokoyama, H. (2007) Two-photon fluorescence bioimaging with an all-semiconductor laser picosecond pulse source. *Opt. Lett.* **32**(18), 2726–2728.
[24] Lichtner, M., Wolfrum, M. & Yanchuk, S. (2011) The spectrum of delay differential equations with large delay. *SIAM J. Math. Anal.* **43**(2), 788–802.
[25] May, R. M. & Anderson, R. M. (1978) Regulation and stability of host-parasite population interactions: II. Destabilizing processes. *J. Anim. Ecol.* **47**(1), 249–267.
[26] Mitchell, J. L. & Carr, T. W. (2010) Oscillations in an intrahost model of plasmodium falciparum malaria due to cross-reactive immune response. *Bull. Math. Biol.* **72**, 590–610.

[27] New, G. H. C. (1974) Pulse evolution in mode-locked quasi-continuous lasers. *IEEE J. Quantum Electron.* **10**(2), 115–124.
[28] Nizette, M., Rachinskii, D., Vladimirov, A. & Wolfrum, M. (2006) Pulse interaction via gain and loss dynamics in passive mode locking. *Phys. D: Nonlinear Phenom.* **218**(1), 95–104.
[29] Pieroux, D. & Erneux, T. (1996) Strongly pulsating lasers with delay. *Phys. Rev. A* **53**, 2765–2771.
[30] Pieroux, D., Erneux, T. & Otsuka, K. (1994) Minimal model of a class-B laser with delayed feedback: Cascading branching of periodic solutions and period-doubling bifurcation. *Phys. Rev. E* **50**, 1822–1829.
[31] Pimenov, A., Habruseva, T., Rachinskii, D., Hegarty, S. P., Guillaume, H. & Vladimirov, A. G. (2014) Effect of dynamical instability on timing jitter in passively mode-locked quantum-dot lasers. *Opt. Lett.* **39**, 6815–6818.
[32] Pimenov, A., Viktorov, E. A., Hegarty, S. P., Habruseva, T., Huyet, G. & Vladimirov, A. G. (2014) Bistability and hysteresis in an optically injected two-section semiconductor laser. *Phys. Rev. E* **89**, 052903.
[33] Puzyrev, D., Vladimirov, A. G., Gurevich, S. V. & Yanchuk, S. (2016) Modulational instability and zigzagging of dissipative solitons induced by delayed feedback. *Phys. Rev. A* **93**, 041801(R).
[34] Pyragas, K. (1992) Continuous control of chaos by self-controlling feedback. *Phys. Lett. A* **170**, 421–428.
[35] Rachinskii, D., Vladimirov, A., Bandelow, U., Hüttl, B. & Kaiser, R. (2006) Q-switching instability in a mode-locked semiconductor laser. *JOSA B* **23**(4), 663–670.
[36] Ruan, S. (2009) On nonlinear dynamics of predator-prey models with discrete delay. *Math. Model. Nat. Phenom.* **4**(02), 140–188.
[37] Schwartz, I. B. & Smith, H. L. (1983) Infinite subharmonic bifurcation in an SEIR epidemic model. *J. Math. Biol.* **18**, 233–253.
[38] Taylor, M. L. & Carr, T. W. (2009) An sir epidemic model with partial temporary immunity modeled with delay. *J. Math. Biol.* **59**, 841–880.
[39] Tuckerman, L. S. & Barkley, D. (1990) Bifurcation analysis of the Eckhaus instability. *Physica D* **46**, 57–86.
[40] Vladimirov, A. G., Rachinskii, D. & Wolfrum, M. (2012) Modeling of passively mode-locked semiconductor lasers. In: K. Lüdge (editor), *Nonlinear Laser Dynamics: From Quantum Dots to Cryptography*, chapter VIII, John Wiley & Sons, Wiley-VCH Verlag GmbH & Co. KGaA. pp. 189–222.
[41] Vladimirov, A. G. & Turaev, D. (2005) Model for passive mode locking in semiconductor lasers. *Phys. Rev. A* **72**(3), 033808.
[42] Vladimirov, A. G., Turaev, D. & Kozyreff, G. (2004) Delay differential equations for mode-locked semiconductor lasers. *Opt. Lett.* **29**(11), 1221–1223.
[43] Vladimirov, A. G. & Turaev, D. V. (2004) A new model for a mode-locked semiconductor laser. *Radiophys. Quantum Electron.* **47**(10–11), 769–776.
[44] Vladimirov, A. G., Wolfrum, M., Fiol, G., Arsenijevic, D., Bimberg, D., Viktorov, E., Mandel, P. & Rachinskii, D. (2010) Locking characteristics of a 40-GHz hybrid mode-locked monolithic quantum dot laser. In: *SPIE Photonics Europe*, International Society for Optics and Photonics, pp. 77200Y–77200Y.
[45] Xu, R., Chaplain, M. A. J. & Davidson, F. A. (2004) Persistence and stability of a stage-structured predator-prey model with time delays. *Appl. Math. Comput.* **150**, 259–277.
[46] Yanchuk, S. & Wolfrum, M. (2006) Eckhaus instability in systems with large delay. *Phys. Rev. Lett.* **6**, 220201.
[47] Yanchuk, S. & Wolfrum, M. (2010) A multiple time scale approach to the stability of external cavity modes in the Lang-Kobayashi system using the limit of large delay. *SIAM J. Appl. Dyn. Syst.* **9**(2), 519–535.